Gamma-Ray Flares from the Crab Nebula

A. A. Abdo, *et al.*

Science **331**, 739 (2011);
DOI: 10.1126/science.1199705

23. C. M. Espinoza *et al.*, *Astronomer's Telegram*, 2889; www.astronomerstelegram.org (2010).
24. J. Arons, in *Neutron Stars and Pulsars, 40 Years After the Discovery*, W. Becker, Ed. (Springer, New York, 2008), pp. 1–56.
25. G. J. Kirk, A. W. Guthmann, Y. A. Gallant, A. Achteberg, *Astrophys. J.* **542**, 235 (2000).
26. A. Spitkovsky, A. Arons, *Astrophys. J.* **603**, 669 (2004).
27. U. Keshet, E. Waxman, *Phys. Rev. Lett.* **94**, 111102 (2005).
28. B. Reville, J. G. Kirk, *Astrophys. J.*, arXiv:1010.0872v1 (2010).
29. Y. A. Gallant, J. Arons, *Astrophys. J.* **435**, 230 (1994).
30. C. A. Wilson-Hodge *et al.*, arXiv:1010.2679v1 (2010).
31. G. Aielli *et al.*, *Astronomer's Telegram*, 2921; www.astronomerstelegram.org (2010).

32. We thank the Chandra Observatory Director H. Tananbaum; HST director M. Mountain; N. Gehrels; and the Swift team for their prompt response in carrying out the observations reported in this paper. Research partially supported by ASI grant I/089/06/2.

Supporting Online Material
www.sciencemag.org/cgi/content/full/science.1200083/DC1
SOM Text
Figs. S1 to S5
Table S1
References

21 October 2010; accepted 13 December 2010
Published online 6 January 2011;
10.1126/science.1200083

Gamma-Ray Flares from the Crab Nebula

A. A. Abdo,[1] M. Ackermann,[2] M. Ajello,[2] A. Allafort,[2] L. Baldini,[3] J. Ballet,[4] G. Barbiellini,[5,6] D. Bastieri,[7,8] K. Bechtol,[2] R. Bellazzini,[3] B. Berenji,[2] R. D. Blandford,[2]* E. D. Bloom,[2] E. Bonamente,[9,10] A. W. Borgland,[2] A. Bouvier,[2] T. J. Brandt,[11,12] J. Bregeon,[3] A. Brez,[3] M. Brigida,[13,14] P. Bruel,[15] R. Buehler,[2]* S. Buson,[7,8] G. A. Caliandro,[16] R. A. Cameron,[2] A. Cannon,[17,18] P. A. Caraveo,[19] J. M. Casandjian,[4] Ö. Çelik,[17,20,21] E. Charles,[2] A. Chekhtman,[22] C. C. Cheung,[1] J. Chiang,[2] S. Ciprini,[10] R. Claus,[2] J. Cohen-Tanugi,[23] L. Costamante,[2] S. Cutini,[24] F. D'Ammando,[25,26] C. D. Dermer,[27] A. de Angelis,[28] A. de Luca,[29] F. de Palma,[13,14] S. W. Digel,[2] E. do Couto e Silva,[2] P. S. Drell,[2] A. Drlica-Wagner,[2] R. Dubois,[2] D. Dumora,[30] C. Favuzzi,[13,14] S. J. Fegan,[15] E. C. Ferrara,[17] W. B. Focke,[2] P. Fortin,[15] M. Frailis,[28,31] Y. Fukazawa,[32] S. Funk,[2]* P. Fusco,[13,14] F. Gargano,[14] D. Gasparrini,[24] N. Gehrels,[17] S. Germani,[9,10] N. Giglietto,[13,14] F. Giordano,[13,14] M. Giroletti,[33] T. Glanzman,[2] G. Godfrey,[2] I. A. Grenier,[4] M.-H. Grondin,[30] J. E. Grove,[27] S. Guiriec,[34] D. Hadasch,[16] Y. Hanabata,[32] A. K. Harding,[17] K. Hayashi,[32] M. Hayashida,[2] E. Hays,[17] D. Horan,[15] R. Itoh,[32] G. Jóhannesson,[35] A. S. Johnson,[2] T. J. Johnson,[17,36] D. Khangulyan,[42] T. Kamae,[2] H. Katagiri,[32] J. Kataoka,[37] M. Kerr,[38] J. Knödlseder,[11] M. Kuss,[3] J. Lande,[2] L. Latronico,[3] S.-H. Lee,[2] M. Lemoine-Goumard,[30] F. Longo,[5,6] F. Loparco,[13,14] P. Lubrano,[9,10] G. M. Madejski,[2] A. Makeev,[22] M. Marelli,[19] M. N. Mazziotta,[14] J. E. McEnery,[17,36] P. F. Michelson,[2] W. Mitthumsiri,[2] T. Mizuno,[32] A. A. Moiseev,[20,36] C. Monte,[13,14] M. E. Monzani,[2] A. Morselli,[39] I. V. Moskalenko,[2] S. Murgia,[2] T. Nakamori,[37] M. Naumann-Godo,[4] P. L. Nolan,[2] J. P. Norris,[40] E. Nuss,[23] T. Ohsugi,[41] A. Okumura,[42] N. Omodei,[2] J. F. Ormes,[40] M. Ozaki,[42] D. Paneque,[2] D. Parent,[22] V. Pelassa,[23] M. Pepe,[9,10] M. Pesce-Rollins,[3] M. Pierbattista,[4] F. Piron,[23] T. A. Porter,[2] S. Rainò,[13,14] R. Rando,[7,8] P. S. Ray,[27] M. Razzano,[3] A. Reimer,[2,43] O. Reimer,[2,43] T. Reposeur,[30] S. Ritz,[44] R. W. Romani,[2] H. F.-W. Sadrozinski,[44] D. Sanchez,[15] P. M. Saz Parkinson,[44] J. D. Scargle,[45] T. L. Schalk,[44] C. Sgrò,[3] E. J. Siskind,[46] P. D. Smith,[12] G. Spandre,[3] P. Spinelli,[13,14] M. S. Strickman,[27] D. J. Suson,[47] H. Takahashi,[41] T. Takahashi,[42] T. Tanaka,[2] J. B. Thayer,[2] D. J. Thompson,[17] L. Tibaldo,[4,7,8] D. F. Torres,[16,48] G. Tosti,[9,10] A. Tramacere,[2,49,50] E. Troja,[17] Y. Uchiyama,[2] J. Vandenbroucke,[2] V. Vasileiou,[20,21] G. Vianello,[2,49] V. Vitale,[39,51] P. Wang,[2] K. S. Wood,[27] Z. Yang,[52,53] M. Ziegler[44]

A young and energetic pulsar powers the well-known Crab Nebula. Here, we describe two separate gamma-ray (photon energy greater than 100 mega–electron volts) flares from this source detected by the Large Area Telescope on board the Fermi Gamma-ray Space Telescope. The first flare occurred in February 2009 and lasted approximately 16 days. The second flare was detected in September 2010 and lasted approximately 4 days. During these outbursts, the gamma-ray flux from the nebula increased by factors of four and six, respectively. The brevity of the flares implies that the gamma rays were emitted via synchrotron radiation from peta–electron-volt (10^{15} electron volts) electrons in a region smaller than 1.4×10^{-2} parsecs. These are the highest-energy particles that can be associated with a discrete astronomical source, and they pose challenges to particle acceleration theory.

The Crab Nebula is the remnant of an historical supernova (SN), recorded in 1054 A.D., located at a distance of 2 kpc (*1*). The SN explosion left behind a pulsar, which continuously emits a wind of magnetized plasma of electron/positron pairs (henceforth referred to as electrons). This pulsar wind is expected to terminate in a standing shock, in which the particles may undergo shock acceleration (*2*, *3*). As the electrons diffuse into the downstream medium, they release energy through interactions with the surrounding magnetic and photon fields. This emission is observed across all wavebands, from radio up to teraelectron-volt gamma-ray energies and is referred to as a pulsar wind nebula (PWN). The efficiency of this process is remarkable. As much as 30% of the total energy released by the Crab pulsar is emitted by the PWN [(*4*) and references therein]. The Crab PWN has an approximately ellipsoidal shape on the sky with a size that decreases with increasing photon energy. At radio frequencies, it extends out to 5′ (3 pc) from the central pulsar. At x-ray wavelengths, a bright torus surrounds the pulsar; its radius is 40″ (0.4 pc), and jets emerge perpendicular to it in both directions.

Within the region encapsulated by the torus, there are several small-scale structures. The inner nebula, which we define as the central 15″ around the pulsar, has several small-scale regions of variable x-ray and optical brightness. The most prominent is an x-ray-bright inner ring with a radius of 10″ (0.1 pc); this ring is thought to represent the termination shock of the PWN (*5*). Several knots with diameters of ~1″ (0.01 pc) are detected close to the inner ring and the base of the jets, and bright arcs of comparable width are observed moving outwards from the inner ring into the torus (*6*, *7*).

The broad-band spectral energy distribution (SED) of the Crab Nebula is composed of two broad nonthermal components. A low-energy component dominates the overall output and extends from radio to gamma-ray frequencies. This emission is thought to be from synchrotron radiation. This notion is confirmed in radio to x-ray frequencies through polarization measurements (*8*–*10*). The emission of this synchrotron component peaks between optical and x-ray frequencies, where the emission is primarily from the torus (*5*). The emission site of higher-energy photons (beyond 100 keV) cannot be resolved because of the limited angular resolution of telescopes that are observing at these frequencies. The high-energy component dominates the emission above ~400 MeV and is thought to be emitted via inverse Compton (IC) scattering, predominantly of the synchrotron photons (*11*, *12*).

The large-scale integrated emission from the Crab Nebula is expected to be steady within a few percent and is thus often used to cross-calibrate x-ray and gamma-ray telescopes and to check their stability over time (*13*, *14*). Recently, variability in the x-ray flux from the nebula by ~3.5% $year^{-1}$ has been detected, setting limits on the accuracy of this practice (*15*). Yearly variations in the emission in the high-energy tail (1 to 150 MeV) of the synchrotron component has also been reported (*16*, *17*). No significant variations have been detected for the high-energy component of the nebula (*18*–*20*).

The Large Area Telescope (LAT) on board the Fermi Gamma-Ray Space Telescope (Fermi) has continuously monitored the Crab Nebula as a

part of its all-sky survey since August 2008. The LAT detects gamma rays from 20 MeV to >300 GeV, and this spans the transition region between the low- and high-energy components of the nebular spectrum. The average SED measured during the first 25 months of observations (Fig. 1) is well characterized by the sum of two spectral components, each with a power-law dependence on energy (*21*). The integrated flux of the low-energy component is $(6.2 \pm 0.3) \times 10^{-7}$ cm^{-2} above 100 MeV, with an photon index of 3.69 ± 0.11 [only statistical errors are given; see supporting online material (SOM) text for a discussion of systematic errors]. The high-energy component has an integral flux of $(1.3 \pm 0.1) \times 10^{-7}$ cm^{-2} s^{-1} above 100 MeV, with a photon index of 1.67 ± 0.04. Because of its hard energy spectrum, the high-energy component dominates the emission above 426 ± 35 MeV.

In order to search for flux variability of both spectral components in the LAT band, we grouped the flux measurements into monthly time bins. The high-energy component was found to be stable. The low-energy component was found to vary on these time scales (Fig. 2); the probability that the measured flux variations are statistical measurement fluctuations in a constant source is less than 10^{-5}. No significant spectral variations were detected for either component on monthly time scales. Flux variability was also searched for on submonthly time scales, for which the low-energy component of the nebula is significantly detected by the LAT only in high-flux states. The flux of the low-energy component was significantly enhanced as compared with the average values in February 2009 and September 2010 (Fig. 2). No variations were found for the high-energy component. The September flare was first announced by the AGILE (Astro–rivelatore Gamma a Immagini Leggero) gamma-ray mission (*22*), which additionally reports a flare in October 2007, before the start of Fermi observations (*23*). The Fermi-LAT–detected flare in February 2009 was not detected by AGILE because the instrument was pointing at a different part of the sky.

The February flare had a duration of ~16 days. The average integral flux above 100 MeV of the low-energy component between Modified Julian Day (MJD) 54857.73 and 54873.73 was $(23.2 \pm 2.9) \times 10^{-7}$ cm^{-2} s^{-1}, corresponding to an increase by a factor 3.8 ± 0.5 compared with the average value; the increase is significant at >8-σ level. The September flare lasted for only ~4 days. The integral flux above 100 MeV between MJD 55457.73 and 55461.73 was $(33.8 \pm 4.6) \times 10^{-7}$ cm^{-2} s^{-1}, corresponding to an increase by a factor 5.5 ± 0.8 with respect to the average and a significance of >10 σ.

The February flare has a soft spectrum with a photon index of 4.3 ± 0.3 (Fig. 1). The spectral slope is compatible with the average 25-month value within 2 SD. The energy spectrum for the second flare was significantly harder, with a photon index of 2.7 ± 0.2, and was still detected above 1 GeV at a 3-σ level. The average power released in each of the gamma-ray flares was approximately 4×10^{36} erg s^{-1}, for the case of isotropic emission. No significant variations in the emission of the pulsar were detected on monthly and 4-day time scales through the period of observations. Examination of the timing residuals of the pulsed emission indicated neither significant variations during either flares nor any significant glitch activity during the first 25 months of LAT observations.

No variations in the synchrotron component between infrared and x-ray frequencies were seen about the average nebular flux level during the second flare (*24*). We analyzed data collected by the Burst Alert Technique (BAT) instrument on board the Swift satellite (*25*), which continuously monitors the sky at photon energies of 15 to 150 keV. The mean flux measured during the first flare was $(2.0 \pm 0.1) \times 10^{-8}$ erg cm^{-2} s^{-1}; the flux during the second flare was $(2.0 \pm 0.1) \times 10^{-8}$ erg cm^{-2} s^{-1}. Both observations are therefore within 5% of the average flux of $(2.09 \pm 0.10) \times 10^{-8}$ erg cm^{-2} s^{-1} measured by BAT in this energy range (*26*) and show no correlation to the gamma-ray flares. The angular resolution of the BAT only allows for the measurement of the spatially integrated spectrum. Sub-arc-second–resolution images were taken in x-rays by the Chandra observatory and optical by the Hubble Space Telescope a few days after the second flare. Although both images show no unusual activity as compared with previous observations, both show a brightening 3″ east of the pulsar (*27*). In the Chandra image, this brightening is associated with a knot of ~1″ diameter that might be associated with the inner ring or the base of the jet. Such a brightening might be interpreted as an afterglow at lower frequencies of the gamma-ray flare, but no conclusions can be drawn on the basis of one event.

The brief flare time scales and the requirement that the emission volume be causally connected imply that the flaring region must have been compact. If L is the diameter of the flaring region along the line of sight and t is the flare duration, then $L < Dct$, where the Doppler factor D accounts for relativistic boosting effects and c is the speed of light. The Doppler factor is expected to be moderate within the Crab Nebula because the typical velocities observed are smaller than 0.9 c (*7*). Even if the emission region was moving directly toward us, this yields $D < 4.4$. For a flare duration of 4 days, this results in $L <$

[1]National Research Council Research Associate, National Academy of Sciences, Washington, DC 20001, USA; Naval Research Laboratory, Washington, DC 20375, USA. [2]W. W. Hansen Experimental Physics Laboratory, Kavli Institute for Particle Astrophysics and Cosmology, Department of Physics and SLAC National Accelerator Laboratory, Stanford University, Stanford, CA 94305, USA. [3]Istituto Nazionale di Fisica Nucleare (INFN), Sezione di Pisa, I-56127 Pisa, Italy. [4]Laboratoire AIM, Commissariat à l'Énergie Atomique (CEA)– Institute of Research into the Fundamental Laws of the Universe (IRFU)/CNRS/Université Paris Diderot, Service d'Astrophysique, CEA Saclay, 91191 Gif sur Yvette, France. [5]INFN, Sezione di Trieste, I-34127 Trieste, Italy. [6]Dipartimento di Fisica, Università di Trieste, I-34127 Trieste, Italy. [7]INFN, Sezione di Padova, I-35131 Padova, Italy. [8]Dipartimento di Fisica "G. Galilei," Università di Padova, I-35131 Padova, Italy. [9]INFN, Sezione di Perugia, I-06123 Perugia, Italy. [10]Dipartimento di Fisica, Università degli Studi di Perugia, I-06123 Perugia, Italy. [11]Centre d'Étude Spatiale des Rayonnements, CNRS/UPS, BP 44346, F-30128 Toulouse Cedex 4, France. [12]Department of Physics, Center for Cosmology and Astro-Particle Physics, Ohio State University, Columbus, OH 43210, USA. [13]Dipartimento di Fisica "M. Merlin" dell'Università e del Politecnico di Bari, I-70126 Bari, Italy. [14]INFN, Sezione di Bari, 70126 Bari, Italy. [15]Laboratoire Leprince-Ringuet, École polytechnique, CNRS/IN2P3, Palaiseau, France. [16]Institut de Ciencies de l'Espai, Institut d'Estudis Espacials de Catalunya–Consejo Superior de Investigaciones Científicas (IEEC-CSIC), Campus UAB, 08193 Barcelona, Spain. [17]NASA Goddard Space Flight Center, Greenbelt, MD 20771, USA. [18]School of Physics, University College Dublin, Belfield, Dublin 4, Ireland. [19]Istituto Nazionale di Astrofisica–Istituto di Astrofisica Spaziale e Fisica Cosmica (INAF-IASF), I-20133 Milano, Italy. [20]Center for Research and Exploration in Space Science and Technology (CRESST) and NASA Goddard Space Flight Center, Greenbelt, MD 20771, USA. [21]Department of Physics and Center for Space Sciences and Technology, University of Maryland Baltimore County, Baltimore, MD 21250, USA. [22]College of Science, George Mason University, Fairfax, VA 22030, USA; Naval Research Laboratory, Washington, DC 20375, USA. [23]Laboratoire de Physique Théorique et Astroparticules, Université Montpellier 2, CNRS/IN2P3, Montpellier, France. [24]Agenzia Spaziale Italiana (ASI) Science Data Center, I-00044 Frascati (Roma), Italy. [25]IASF Palermo, 90146 Palermo, Italy. [26]INAF-IASF, I-00133 Roma, Italy. [27]Space Science Division, Naval Research Laboratory, Washington, DC 20375, USA. [28]Dipartimento di Fisica, Università di Udine and Istituto Nazionale di Fisica Nucleare, Sezione di Trieste, Gruppo Collegato di Udine, I-33100 Udine, Italy. [29]Istituto Universitario di Studi Superiori (IUSS), I-27100 Pavia, Italy. [30]Université Bordeaux 1, CNRS/IN2p3, Centre d'Études Nucléaires de Bordeaux Gradignan, 33175 Gradignan, France. [31]Osservatorio Astronomico di Trieste, Istituto Nazionale di Astrofisica, I-34143 Trieste, Italy. [32]Department of Physical Sciences, Hiroshima University, Higashi-Hiroshima, Hiroshima 739-8526, Japan. [33]INAF–Istituto di Radioastronomia, 40129 Bologna, Italy. [34]Center for Space Plasma and Aeronomic Research (CSPAR), University of Alabama in Huntsville, Huntsville, AL 35899, USA. [35]Science Institute, University of Iceland, IS-107 Reykjavik, Iceland. [36]Department of Physics and Department of Astronomy, University of Maryland, College Park, MD 20742, USA. [37]Research Institute for Science and Engineering, Waseda University, 3-4-1, Okubo, Shinjuku, Tokyo, 169-8555 Japan. [38]Department of Physics, University of Washington, Seattle, WA 98195–1560, USA. [39]INFN, Sezione di Roma "Tor Vergata," I-00133 Roma, Italy. [40]Department of Physics and Astronomy, University of Denver, Denver, CO 80208, USA. [41]Hiroshima Astrophysical Science Center, Hiroshima University, Higashi-Hiroshima, Hiroshima 739-8526, Japan. [42]Institute of Space and Astronautical Science, Japan Aerospace Exploration Agency (JAXA), 3-1-1 Yoshinodai, Chuo-ku, Sagamihara, Kanagawa 252-5210, Japan. [43]Institut für Astro- und Teilchenphysik and Institut für Theoretische Physik, Leopold-Franzens-Universität Innsbruck, A-6020 Innsbruck, Austria. [44]Santa Cruz Institute for Particle Physics, Department of Physics and Department of Astronomy and Astrophysics, University of California at Santa Cruz, Santa Cruz, CA 95064, USA. [45]Space Sciences Division, NASA Ames Research Center, Moffett Field, CA 94035–1000, USA. [46]NYCB Real-Time Computing, Lattingtown, NY 11560–1025, USA. [47]Department of Chemistry and Physics, Purdue University Calumet, Hammond, IN 46323–2094, USA. [48]Institució Catalana de Recerca i Estudis Avançats (ICREA), Barcelona, Spain. [49]Consorzio Interuniversitario per la Fisica Spaziale (CIFS), I-10133 Torino, Italy. [50]INTEGRAL Science Data Centre, CH-1290 Versoix, Switzerland. [51]Dipartimento di Fisica, Università di Roma "Tor Vergata," I-00133 Roma, Italy. [52]Department of Physics, Stockholm University, AlbaNova, SE-106 91 Stockholm, Sweden. [53]The Oskar Klein Centre for Cosmoparticle Physics, AlbaNova, SE-106 91 Stockholm, Sweden.

*To whom correspondence should be addressed. E-mail: buehler@stanford.edu (R.B.); rdb3@stanford.edu (R.D.B.); funk@slac.stanford.edu (S.F.)

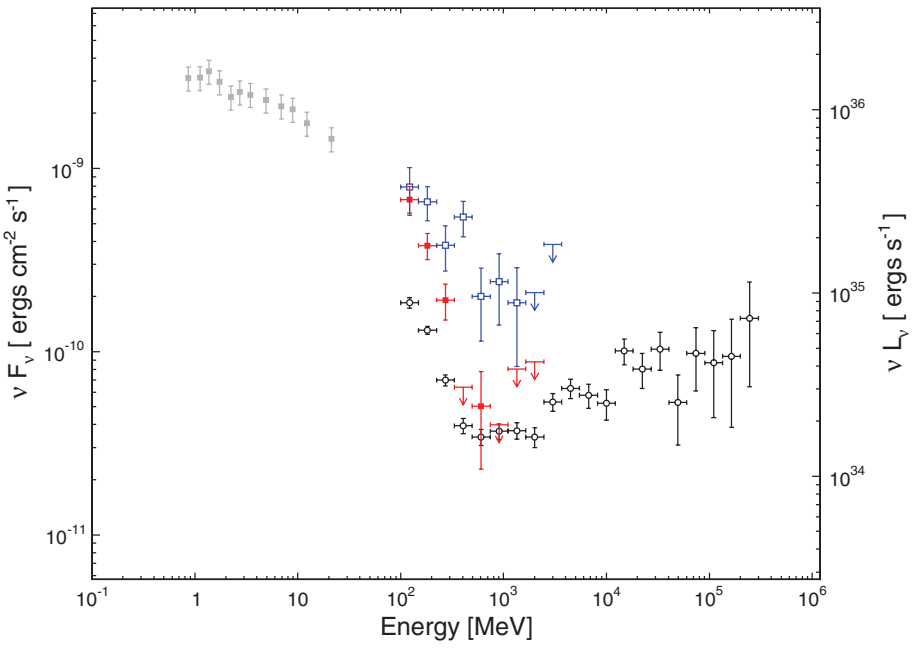

Fig. 1. Spectral energy distribution of the Crab Nebula. Black open circles indicate the average spectrum measured by the LAT in the first 25 months of observations. Red squares indicate the energy spectrum during the flare of February 2009 (MJD 54857.73 to 54873.73), and blue open squares indicate the spectrum in September 2010 (MJD 55457.73 to 55461.73). Gray squares indicate historical long-term average spectral data from the COMPTEL telescope, with 15% systematic errors (*41*). Arrows indicate 95% confidence flux limits.

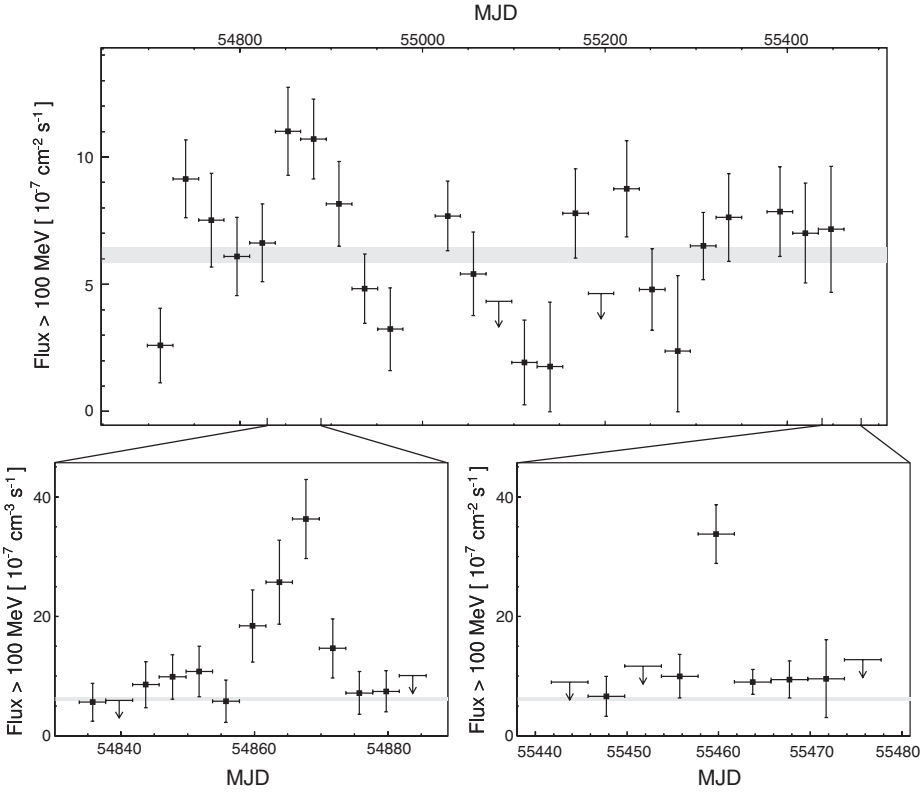

Fig. 2. Gamma-ray flux above 100 MeV as a function of time of the synchrotron component of the Crab Nebula. (**Top**) The flux in four-week intervals for the first 25 month of observations. Data for times when the sun was within 15° of the Crab Nebula have been omitted. The gray band indicates the average flux measured over the entire period. (**Bottom**) The flux as a function of time in 4-day time bins during the flaring periods in February 2009 and September 2010. Arrows indicate 95% confidence flux limits.

1.4×10^{-2} pc, which corresponds to < 1.5″ projected on the sky. Structures this small are found only in the inner part of the nebula—close to the termination shock, the base of the jet, or the pulsar—suggesting that the gamma-ray emission detected in the flare originated from these regions. This is in agreement with expectations of relativistic magnetohydrodynamic simulations, in which the gamma-ray emission of the synchrotron component originates close to the termination shock (*28*, *29*).

The extrapolation of the the LAT spectrum of low-energy component to lower frequencies suggest that it represents synchrotron emission (Fig. 1). The brevity of the gamma-ray flares strengthens this scenario: If the flare were instead produced by IC radiation or Bremsstrahlung, the cooling time of the emitting electrons would greatly exceed the flare duration. The cooling via Bremsstrahlung in particle densities of <10 cm^{-3} (*30*) happens over ~10^6 years. Similarly, electrons cooling via IC emission of 100 MeV gamma rays on the photons of the synchrotron component of Crab Nebula have cooling times of $\gtrsim 10^7$ years. The average magnetic field inside the Crab Nebula is estimated to be ~200 μG, as deduced from modeling of the broad-band SED (*12*, *21*), and might be enhanced locally by up to an order of magnitude in the inner nebula (*31*). These fields imply synchrotron cooling times $\lesssim$15 days, which is comparable with the flare duration, leaving synchrotron radiation as the only plausible process responsible for the gamma-ray emission during the flares.

The detection of synchrotron photons up to energies of >1 GeV confirms that electrons are accelerated to energies of ≥1 PeV in the Crab Nebula (*32*). These are the highest-energy particles that can be associated directly with any astronomical source, and they pose special challenges to particle acceleration theory. Because synchrotron losses are so efficient, there must be a strong electric field E to compensate radiation reaction, given by

$$E/B \approx r_L/l_{cool} \geq (1.3\alpha E_{\gamma pk}/m_e c^2) \approx (E_{\gamma pk}/50\ \mathrm{MeV}) \quad (1)$$

where r_L is the Larmor radius, l_{cool} is the radiative cooling length, α is the fine structure constant, m_e is the electron mass, and $E_{\gamma pk}$ is the peak synchrotron frequency at which the most energetic electrons are emitting (*33*, *17*). Because of the detection of gamma-ray emission beyond 1 GeV, $E_{\gamma pk}$ can be conservatively estimated to be >200 MeV. The electric field is unlikely to exceed the magnetic field; if it did, there would be a local reference frame with a pure electric field in which vacuum breakdown would occur quickly. We conclude that the electric field, as measured in the Crab frame, is close in magnitude to the magnetic field in the region where the highest-energy synchrotron photons were emitted. This subsumes the possibility of bulk relativistic motion. Furthermore, the resistive force due to radiation reaction is

competitive with the Lorentz force, and the cooling length is comparable with the Larmor radius. This poses severe difficulties to the widely discussed acceleration mechanism of diffusive shock acceleration (*34*, *35*). The proposed acceleration due to absorption of ion cyclotron waves does not suffer from these constraints (*36*). However, it appears to operate on time scales that are too long to accommodate the fast variability seen during the flares. Alternatively, the acceleration could be related directly to the electric field from the pulsar.

The Crab Nebula is powered by the central neutron star, which acts as a dc unipolar inductor and a source of an ac-striped wind (*2*, *3*). What happens to the dc and ac current flows is controversial. It is widely supposed that ~90% of the dc current returns in an outflowing wind that becomes particle-dominated and encounters a (mostly invisible) termination shock at a radius ~0.1 pc (*37*), but the wind could also remain electromagnetically dominated (*38*, *33*). For the measured spin-down rate, a moment of inertia of $\sim 1 \times 10^{45}$ g cm^2, and a force-free model of the magnetosphere, the total induced potential difference is ~50 PV, which is high enough to accelerate particles to the required energies. The current associated with this potential is ~300 TA, yielding a dc power per hemisphere of $\sim 1.5 \times 10^{38}$ erg s^{-1}, which is a factor ~40 larger than the power released in the flares. Another interesting possibility is that particle acceleration takes place in the ac-striped wind of the pulsar because of magnetic reconnection, although it is not clear whether this process can accelerate particles to PeV energies on the required time scales (*39*, *40*).

The observations reported here have raised compelling questions on our understanding of particle acceleration and motivate more detailed calculations; together with the ongoing gamma-ray observations of the LAT and observational campaigns at x-ray and optical wavelengths, they might soon pinpoint the gamma-ray emission site in the Crab Nebula.

References and Notes

1. V. Trimble, *Publ. Astron. Soc. Pac.* **85**, 579 (1973).
2. M. J. Rees, J. E. Gunn, *Mon. Not. R. Astron. Soc.* **167**, 1 (1974).
3. C. F. Kennel, F. V. Coroniti, *Astrophys. J.* **283**, 710 (1984).
4. J. J. Hester, *Annu. Rev. Astron. Astrophys.* **46**, 127 (2008).
5. M. C. Weisskopf *et al.*, *Astrophys. J.* **536**, L81 (2000).
6. J. D. Scargle, *Astrophys. J.* **156**, 401 (1969).
7. J. J. Hester *et al.*, *Astrophys. J.* **577**, L49 (2002).
8. W. J. Cocke, M. J. Disney, G. W. Muncaster, T. Gehrels, *Nature* **227**, 1327 (1970).
9. R. Novick *et al.*, *Astrophys. J.* **174**, L1 (1972).
10. A. J. Dean *et al.*, *Science* **321**, 1183 (2008).
11. R. J. Gould, G. R. Burbidge, *Ann. Astrophys.* **28**, 171 (1965).
12. A. M. Atoyan, F. A. Aharonian, *Mon. Not. R. Astron. Soc.* **278**, 525 (1996).
13. M. C. Weisskopf *et al.*, *Astrophys. J.* **713**, 912 (2010).
14. M. Meyer, D. Horns, H. S. Zechlin, http://adsabs.harvard.edu/abs/2010arXiv1008.4524M (2010).
15. C. A. Wilson-Hodge *et al.*, http://adsabs.harvard.edu/abs/2010arXiv1010.2679W (2010).
16. R. Much *et al.*, *Astron. Astrophys.* **299**, 435 (1995).
17. O. C. de Jager *et al.*, *Astrophys. J.* **457**, 253 (1996).
18. F. Aharonian *et al.*, *Astrophys. J.* **614**, 897 (2004).
19. F. Aharonian *et al.*, *Astron. Astrophys.* **457**, 899 (2006).
20. J. Albert *et al.*, *Astrophys. J.* **674**, 1037 (2008).
21. A. A. Abdo *et al.*, *Astrophys. J.* **708**, 1254 (2010).
22. *Astronomer's Telegram*, 2855; www.astronomerstelegram.org (2010).
23. M. Tavani *et al.*, *Science* **331**, 736 (2010).
24. *Astronomer's Telegram*, 2867, 2872, 2893; www.astronomerstelegram.org (2010).
25. M. Ajello *et al.*, *Astrophys. J.* **673**, 96 (2008).
26. BAT digest, http://heasarc.gsfc.nasa.gov/docs/swift/analysis/bat_digest.html.
27. *Astronomer's Telegram*, 2882, 2903; www.astronomerstelegram.org (2010).
28. D. Volpi, L. D. Zanna, E. Amato, N. Bucciantini, *Astron. Astrophys.* **485**, 337 (2008).
29. S. S. Komissarov, M. Lyutikov, http://adsabs.harvard.edu/abs/2010arXiv1011.1800K (2010).
30. A. M. Atoyan, F. A. Aharonian, *Astron. Astrophys. Suppl. Ser.* **120**, 453 (1996).
31. J. J. Hester *et al.*, *Astrophys. J.* **448**, 240 (1995).
32. O. C. de Jager, A. K. Harding, *Astrophys. J.* **396**, 161 (1992).
33. M. Lyutikov, *Mon. Not. R. Astron. Soc.* **405**, 1809 (2010).
34. Y. A. Gallant, *Springer Lect. Notes Phys.* **589**, 24 (2002).
35. L. Sironi, A. Spitkovsky, *Astrophys. J.* **698**, 1523 (2009).
36. E. Amato, J. Arons, *Astrophys. J.* **653**, 325 (2006).
37. N. Bucciantini, J. Arons, E. Amato, *Mon. Not. R. Astron. Soc.* **410**, 381 (2010).
38. *Lighthouses of the Universe: The Most Luminous Celestial Objects and Their Use for Cosmology*, M. Gilfanov, R. Sunyeav, E. Churazov, Eds. (2002).
39. Y. Lyubarsky, M. Liverts, *Astrophys. J.* **682**, 1436 (2008).
40. W. Bednarek, W. Idec, http://adsabs.harvard.edu/abs/2010arXiv1011.4176B (2010).
41. L. Kuiper *et al.*, *Astron. Astrophys.* **378**, 918 (2001).

42. The Fermi LAT Collaboration acknowledges support from a number of agencies and institutes for both development and the operation of the LAT as well as scientific data analysis. These include NASA and the U.S. Department of Energy in the United States; CEA/IRFU and IN2P3/CNRS in France; ASI and INFN in Italy; the Ministry of Education, Culture, Sports, Science and Technology, High Energy Accelerator Research Organization (KEK), and JAXA in Japan; and the K. A. Wallenberg Foundation, the Swedish Research Council, and the National Space Board in Sweden. Additional support from INAF in Italy and CNES in France for science analysis during the operations phase is also gratefully acknowledged. L.T. was partially supported by the International Doctorate on Astroparticle Physics program.

Supporting Online Material

www.sciencemag.org/cgi/content/full/science.1199705/DC1
SOM Text

28 October 2010; accepted 20 December 2010
Published online 6 January 2010;
10.1126/science.1199705

Negative Linear Compressibility and Massive Anisotropic Thermal Expansion in Methanol Monohydrate

A. Dominic Fortes,[1,2]* Emmanuelle Suard,[3] Kevin S. Knight[4,5]

The vast majority of materials shrink in all directions when hydrostatically compressed; exceptions include certain metallic or polymer foam structures, which may exhibit negative linear compressibility (NLC) (that is, they expand in one or more directions under hydrostatic compression). Materials that exhibit this property at the molecular level—crystalline solids with intrinsic NLC—are extremely uncommon. With the use of neutron powder diffraction, we have discovered and characterized both NLC and extremely anisotropic thermal expansion, including negative thermal expansion (NTE) along the NLC axis, in a simple molecular crystal (the deuterated 1:1 compound of methanol and water). Apically linked rhombuses, which are formed by the bridging of hydroxyl-water chains with methyl groups, extend along the axis of NLC/NTE and lead to the observed behavior.

The water-methanol binary system is of importance in biological and industrial chemistry [for example, as an inhibitor of clathrate formation in gas pipelines (*1*)] and is also of interest to cosmochemists studying ice-grain reactions in the interstellar medium and the source of carbon in comets and other primitive solar nebula materials (*2*–*4*). Moreover, methanol may be an important constituent of aqueous cryovolcanic solutions (along with ammonia) on the icy satellites of our solar system (*5*, *6*). As part of a program of study into icy materials in the outer solar system, we have been engaged in measurement and analysis of the structure and properties of compounds containing simple alcohols, water, and ammonia as a function of pressure and temperature (*7*–*10*). In most cases, the difficulty of growing single crystals, due to the high viscosity of the liquid at low temperatures with the concomitant tendency to supercool and form a glass, has meant that structures must be determined from powder diffraction data. In the case of methanol monohydrate, we determined the structure of the perdeuterated isotopologue, $CD_3OD{\cdot}D_2O$, from powder data and discovered a high degree of directionality to the structural elements (*7*).

Neutron powder diffraction measurements were carried out on the high-resolution powder diffractometer (HRPD) (*11*) at the ISIS facility (Rutherford Appleton Laboratory, Oxfordshire, UK) and on the D1A diffractometer (*12*) at the Institut Laue Langevin (Grenoble, France). At the former,

[1]Department of Earth Sciences, University College London (UCL), Gower Street, London WC1E 6BT, UK. [2]Centre for Planetary Sciences at UCL/Birkbeck, Gower Street, London WC1E 6BT, UK. [3]Institut Laue-Langevin (ILL), BP156, 38042 Grenoble cedex 9, France. [4]ISIS Facility, Science and Technology Facilities Council (STFC) Rutherford Appleton Laboratory, Harwell Science and Innovation Campus, Chilton, Didcot, Oxfordshire OX11 0QX, UK. [5]The Natural History Museum, Cromwell Road, London SW7 5BD, UK.

*To whom correspondence should be addressed. E-mail: andrew.fortes@ucl.ac.uk